Supplementary Material (ESI) for *Soft Matter*

Supporting information

Growth mechanism of nanostructured superparamagnetic rods obtained by electrostatic co-assembly

M. Yan[a], J. Fresnais[b] and J.-F. Berret[a]*

[a]Matière et Systèmes Complexes, UMR 7057 CNRS Université Denis Diderot Paris-VII, Bâtiment Condorcet, 10 rue Alice Domon et Léonie Duquet, 75205 Paris (France)
[b]UPMC Paris VI – Laboratoire de Physico-chimie des Electrolytes, Colloïdes et Sciences Analytiques UMR 7195 CNRS 4 place Jussieu, 75252 Paris Cedex 05 (France)

Outline

Movie#1: Rotation of the rod made from NP6.7 in anti-clockwise sense at 30 rpm induced by a home-made device producing a rotating magnetic field of 13 mT at 0.2 Hz.
Movie#2: An external magnetic field of varying magnitude (B = 0 – 12 mT) was applied to the loose and flexible wire-like aggregate resulted from weak electrostatic interactions between NPs. The aggregate could be stretched and elongated by the application of a magnetic field. After removing the field, the stretched structure returned to its initial wire-like state.
Movie#3: An external magnetic field of varying magnitude (B = 0 – 12 mT) was applied to the wire-like aggregate resulted from weak NP initial weight concentration (6×10^{-3} wt. %). The field was progressively increased from B = 0 to 12 mT and the wire-like conformation remained unchanged. Within the optical microscopy accuracy (~ 0.5 μm), the aggregates could not be stretched nor elongated by the application of a field.

SI-1 – Characterization of nanoparticle sizes and size distribution

SI-1.1 – Vibrating sample magnetometry (VSM)

Vibrating sample magnetometry (VSM) consisted in measuring the magnetization *versus* excitation *M(H)* for a solution at volume fraction ϕ from the signal induced in detection coils when the sample is moved periodically in an applied magnetic field (thanks to synchronous detection and with an appropriate calibration). Here we used the superparamagnetic NPs having two dominant populations (sample code: NP6.7 and NP8.3) as a comparison. Fig. S1 shows the evolution of the macroscopic magnetization *M(H)* normalized by its saturation value M_S for the γ-Fe_2O_3 superparamagnetic NP. Here, $M_S = \phi\, m_S$, where m_S is the specific magnetization of colloidal maghemite ($m_S = 3.5\times10^5$ A m^{-1}) which is lower than for bulk maghemite and decrease when the diameters of the superparamagnetic NP decrease due to some disorder of the magnetic moments located near the surface. The solid curve in Fig. S1 was obtained using the Langevin function for superparamagnetism convoluted with a log-normal distribution function of the particle size. The parameters of the distribution are the median diameter ($D_0^{VSM} = 6.7 \pm 0.1$ nm, $D_0^{VSM} = 8.3 \pm 0.1$ nm) and the polydispersity ($s^{VSM} = 0.21 \pm 0.03$, $s^{VSM} = 0.21 \pm 0.02$).

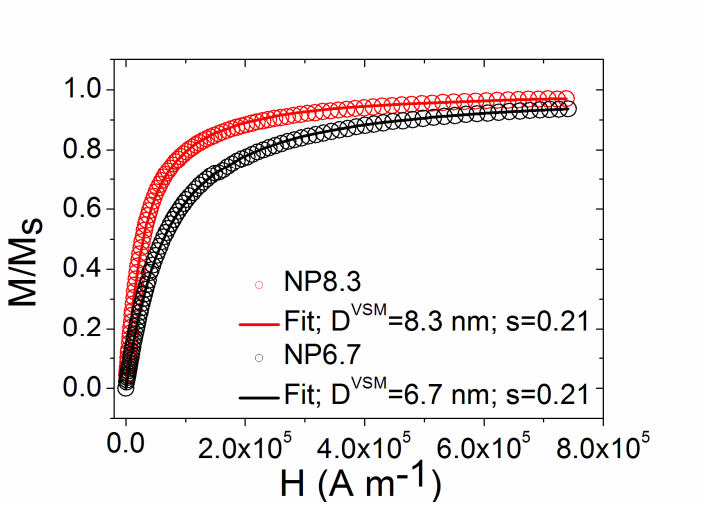

Figure S1 : Magnetic field dependence of the macroscopic magnetization *M(H)* normalized by its saturation value M_S for cationic maghemite dispersions. The solid curve was obtained using the Langevin function for superparamagnetism convoluted with a log-normal distribution function for the particle sizes, given with median diameters D_0^{VSM} and polydispersity s^{VSM}.

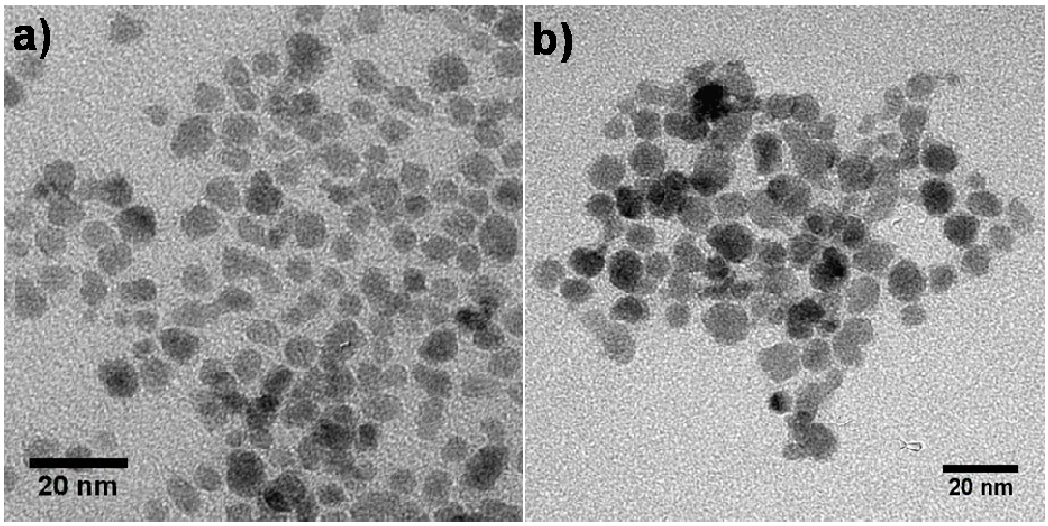

Figure S2 : Iron oxide superparamagnetic NPs. (a) NP6.7 and (b) NP8.3 as observed by TEM. The stability of the dispersion was ensured by electrostatic interactions mediated by the native cationic charges.

SI-1.2 – Transmission Electron Microscopy (TEM)

In fact, the median diameter D_0^{VSM} obtained by VSM is due to the crystal structure inside the γ-Fe_2O_3 nanoparticle. We then compared these values with the physical diameters D_0^{TEM} by using the transmission electron microscopy (TEM). Fig. S2 displays image of the γ-Fe_2O_3 superparamagnetic NPs (NP6.7 and NP8.3).

Probability distribution functions of size for these superparamagnetic NPs observed by TEM on a series of images similar to that of Fig. S2 were shown in Fig. S3. The data could be fitted using a log-normal function with physical diameter D_0^{TEM} = 6.8 ± 0.2 nm, D_0^{TEM} = 9.3 ± 0.2 nm and polydispersity s^{TEM} = 0.21 ± 0.01, s^{TEM} = 0.18 ± 0.01.

$$p(D, D_0, s_D) = \frac{1}{\sqrt{2\pi}\beta_D(s_D)D}\exp\left(-\frac{\ln^2(D/D_0)}{2\beta_D(s_D)^2}\right) \qquad \text{SI(1)}$$

These values were found to be in relative good agreement with the ones obtained from VSM, albeit with a minor difference between the median diameter D_0^{VSM} and physical diameter D_0^{TEM}, which could originate from defects located close to the particle surfaces, and that would not contribute to magnetic properties.

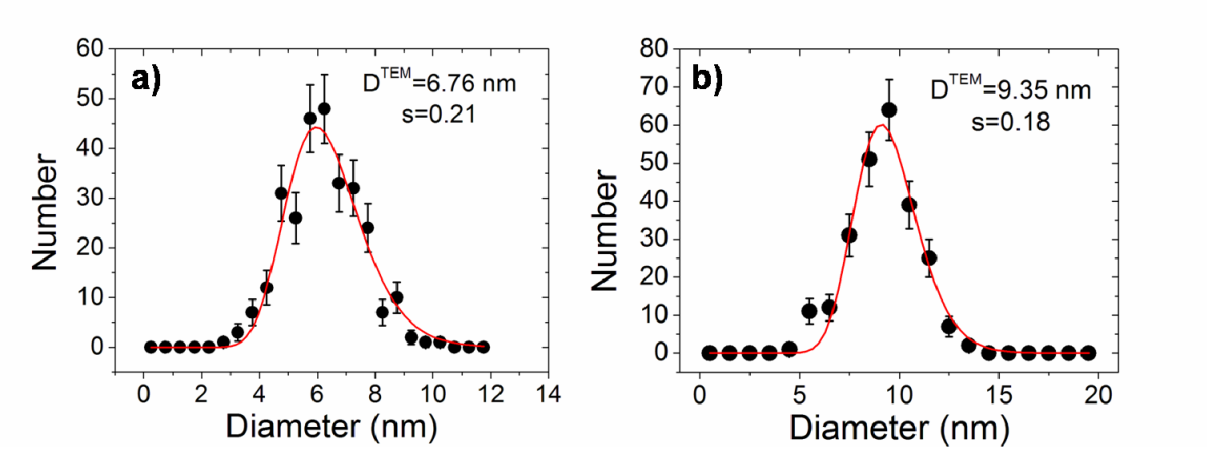

Figure S3 : Probability distributions function of size for the γ-Fe_2O_3 superparamagnetic nanoparticles. (a) : NP6.7 a) and (b) : NP8.3. The continuous line was derived from best fit calculation using a log-normal distribution. For these dispersions, the average size of the superparamagnetic NPs were found to be 6.8 nm and 9.3 nm, and the polydispersity 0.21 and 0.18.

SI-1.3 – Dynamic Light Scattering (DLS)

Dynamic light scattering (DLS) were performed on a Brookhaven spectrometer (BI-9000AT autocorrelator, λ = 632.8 nm) for measurements of the Rayleigh ratio $R(q, c)$ and of the collective diffusion constant $D(c)$. With dynamical light scattering, the collective diffusion coefficient D was determined from the second-order autocorrelation function of the scattered light. From the value of the coefficient, the hydrodynamic diameter of the colloids was calculated according to the Stokes-Einstein relation, $D_H = k_BT/3\pi\eta_SD$, where k_B is the Boltzmann constant, T the temperature (T = 298 K) and η_0 the solvent viscosity ($\eta_S = 0.89\times10^{-3}$ Pa s for water). The autocorrelation functions were interpreted using the cumulants and the CONTIN fitting procedure provided by the instrument software.

With dynamic light scattering, a single mode in the autocorrelation function was observed, corresponding to a hydrodynamic diameter D_H = 14 ± 1 nm, D_H = 17 ± 1 nm and polydispersity index of 0.21. It should be mentioned here that the hydrodynamic sizes appear larger than those determined by TEM or VSM. The reasons for that are well-known. They are: *i)* The particles are distributed in sizes; *ii)* the particles are slightly anisotropic (aspect ratio 0.8); iii) when particles are distributed, light scattering is sensitive to the largest particles of the distribution. The shift between 6 – 7 nm to 6.7 nm and 8 – 9 nm to 8.3 nm is thus fully normal for this type of systems.

SI-2 – Characterization of the nanostructured rods

Fig. S4 displays the length distribution of the rods obtained with the 6.7 nm-particles (NP6.7) and the 8.3 nm-particles (NP8.3). The data were fitted by a log-normal distribution function (Eq. 1) with median length L_0 = 8.2 ± 0.7 and 17.5 ± 0.9 µm for NP6.7 and NP8.3 respectively, and a polydispersity s = 0.50. These data are reported in the main text.

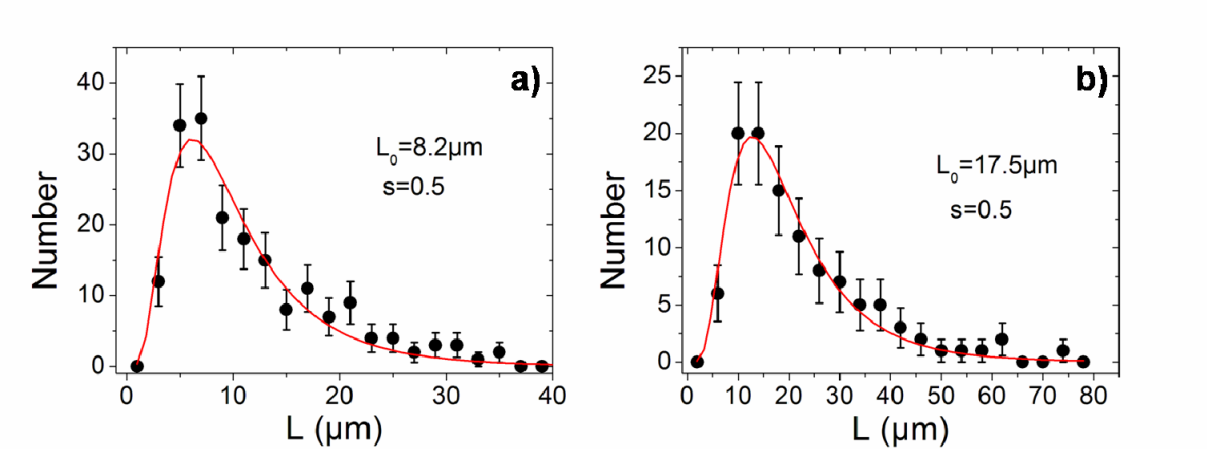

Figure S4 : Length distribution of rods obtained with NP6.7 a) and NP8.3 b). The continuous line was derived from best fit calculation using a log-normal distribution.

SI-3 – Study of rod growth on sample NP8.3 as a function of dialysis time

The microscopy observations of the NP/polymer dispersions (sample NP8.3, c = 0.1 wt. %) in Figs. S5 were carried out in the absence of a magnetic field. In a first period, comprised between the starting of the dialysis and t = 10 mn no microscopic aggregates could be observed (Fig. S5a). One minute later (t = 11 mn), elongated and tortuous structures, hereafter dubbed wire-like aggregates with contour length of a few microns showed up (Fig. S5b). As time evolved (t = 15 and 50 mn), linear and stiff nanostructured rods were finally observed (Figs. S5c and S5d).

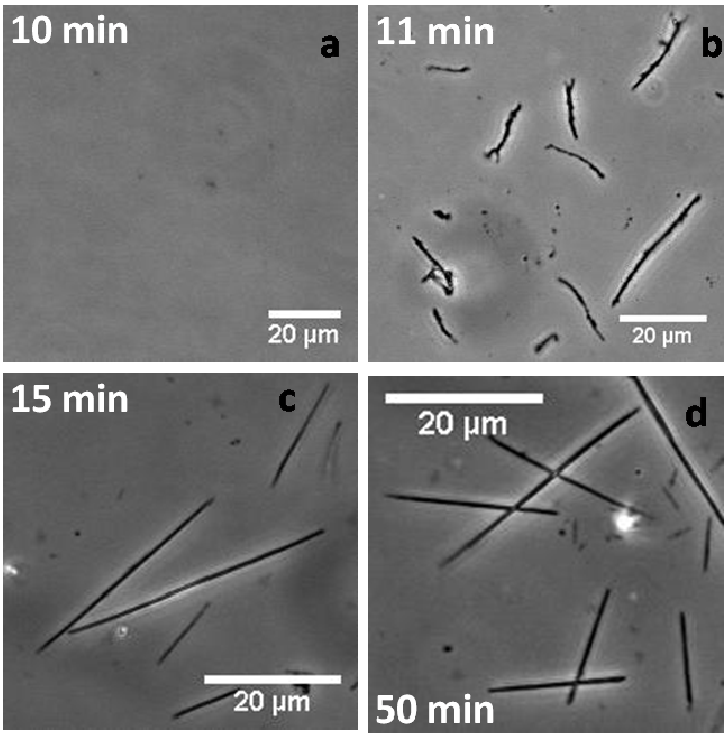

Figure S5 : Phase-contrast optical microscopy images (40×) of the NP/polymer dispersions (sample NP8.3, c = 0.1 wt. %) at time t = 10 a), 11 b), 15 c) and 50 mn d).

SI-4 – Study of rod growth on sample NP8.3 as a function of NP initial weight concentration

Figs. S6 display images of the NP/polymer dispersions (sample NP8.3, dialysis time was fixed at 1 hour) corresponding to the different NP initial weight concentration. At very low concentration, *i.e.* below 10^{-3} wt. %, no supracolloidal aggregates could be observed. For $c = 10^{-3} – 10^{-2}$ wt. %, wire-like aggregates with median contour length of a few microns were observed. Their morphologies were very similar to those obtained by varying the ionic strength or dialysis time. Above a transition concentration $c^* = 10^{-2}$ wt. %, the morphology became that of linear and rigid rods with lengths comprised between 1 and 100 µm.

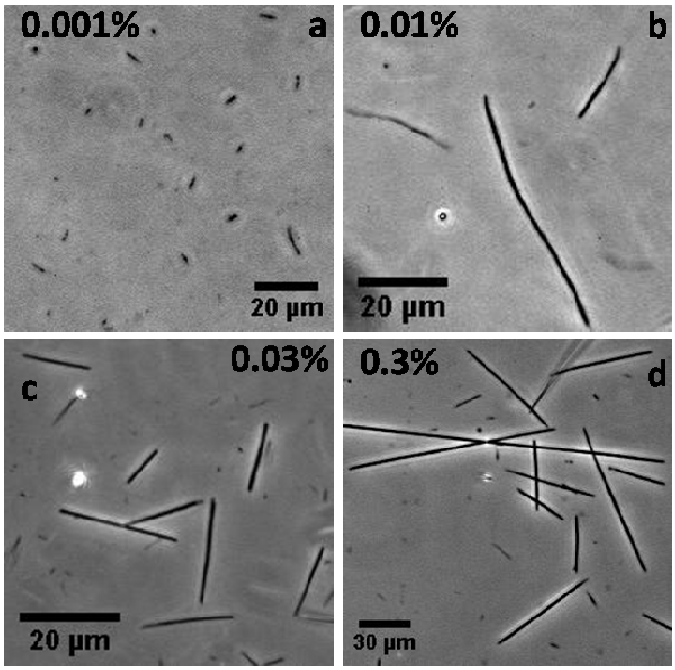

Figure S6 : Phase-contrast optical microscopy images (40×) of the NP/polymer dispersions (sample NP8.3, dialysis time was fixed at 1 hour) corresponding to the different NPs initial weight concentration: 10^{-3} wt. % (a), 10^{-2} wt. % (b), 3×10^{-2} wt. % (c) and 3×10^{-1} wt. % (d).